Constructing Carbon-Coated Fe_3O_4 Microspheres as Antiacid and Magnetic Support for Palladium Nanoparticles for Catalytic Applications

Lirong Kong, Xiaofeng Lu,* Xiujie Bian, Wanjin Zhang, and Ce Wang*

Alan G. MacDiarmid Institute, Jilin University, Changchun 130012, P.R. China

ABSTRACT Fe_3O_4 microsphere is a good candidate as support for catalyst because of its unique magnetic property and large surface area. Coating Fe_3O_4 microspheres with other materials can protect them from being dissolved in acid solution or add functional groups on their surface to adsorb catalyst. In this paper, a carbon layer was coated onto Fe_3O_4 microspheres by hydrothermal treatment using polyethylene glycol as the connecting agents between glucose and Fe_3O_4 spheres. Through tuning the added amounts of reactants, the thickness of the carbon layer could be well-controlled. Because of the abundant reductive groups on the surface of carbon layer, noble metal ions could be easily adsorbed and in situ reduced to nanoparticles (6−12 nm). The prepared catalyst not only had unique antiacid and magnetic properties, but also exhibited a higher catalytic activity toward the reduction of methyl orange than commercially used Pd/C catalyst.

KEYWORDS: coating • functional composites • nanocomposites • environmental degradation • magnetic properties

1. INTRODUCTION

Recently, there is an increasing amount of interests in fabricating nano/micrometer-scale carriers that have important applications in life and materials science (1). Among them, Fe_3O_4 spheres are a promising candidate for their unique magnetic response, large surface area, and low cytotoxicity (2−6). Though Fe_3O_4 spheres have many advantages as a kind of magnetic carriers, people still find that there are two limitations in their practical application. One is that Fe_3O_4 spheres can not be used in strong acidic solution. As reported by our group, the Fe_3O_4 microspheres could be absolutely dissolved after being ultrasonicated in 1 M hydrochloric acid (HCl) for 1 h even after they were coated by a layer of conducting polymers (7). The other important limitation is that Fe_3O_4 microspheres have few functional groups on their surface. As is well-known, the support for drug or catalyst must have abundant functional groups on its surface to adsorb the drug or catalyst. However, pure Fe_3O_4 spheres can hardly adsorb the drugs or catalysts. Considering the above two limitations, people have to coat Fe_3O_4 spheres with other materials to protect them from being dissolved in acid environment and add functional groups on their surface. Among them, silica has being mostly used as the coating material because it can efficiently inhibit the hydrogen ions to get through (8, 9). However, inorganic silica shells also have few functional groups on their surface and must be chemically modified before being used as support for catalyst (2). The modification process is usually inconvenient for industrial application and the modificative agents such as 3-aminopropyl-triethoxysilane are usually toxic, which limit their application in drug delivery, catalyzing the degradation of water pollutants and other processes related to life science. In addition, various polymers, such as polypyrrole and polyaniline, have also been used as the coating material for Fe_3O_4 spheres (7, 10). Though there are always a plenty of functional groups on their surface, the gaps in the network of polymers may allow the hydrogen ions to get through and dissolve the Fe_3O_4 cores. Therefore, it is not very appropriate to use such polymers as the coating material for Fe_3O_4 spheres.

Recently, a new carbon material has aroused many interests because it is prepared by the hydrothermal treatment of low-cost glucose (11−13). The preparative process belongs to "green chemistry" because the reactant is safe and the preparative process causes no contamination to the environment. Moreover, according to the research about glucose-based carbon spheres (12), during the hydrothermal process, glucose was first polymerized in water, and then formed small spheres. After the spheres were formed, they began to carbonize along with being coated with newly formed polysaccharide. Finally, the carbon spheres formed the structure of inner dense carbon layer and outer polysaccharide layer. The carbon layer can efficiently protect the Fe_3O_4 spheres from being dissolved in acid environment because its dense structure can inhibit the hydrogen ions to get through. Moreover, the outer polysaccharide layer offers a great many functional groups, such as carboxylic, aldehyde, and hydroxyl groups, on their surface. Therefore, catalytic noble metal nanoparticles (NPs) can be easily

* Corresponding author. Tel.: +86-431-85168292. Fax: +86-431-85168292. E-mail: xflu@jlu.edu.cn; cwang@jlu.edu.cn.
Received for review August 27, 2010 and accepted November 29, 2010
DOI: 10.1021/am101077a

loaded on them. Considering the above advantages, many groups have tried to coat Fe_3O_4 spheres or NPs with glucose-based carbon layer. Wang et al. used oleic-acid-decorated Fe_3O_4 NPs as the core of Fe_3O_4/carbon spheres (14). Zhang et al. reported the fabrication of functional 1D magnetic NPs chains with thin carbon coatings by using urea as the surfactant (15). However, the size uniformity and the thickness of carbon layer still need to be better controlled and its application as catalyst support needs to be investigated.

In our work, we successfully prepared carbon-coated Fe_3O_4 (Fe_3O_4@C) microspheres by using environmentally friendly surfactant polyethylene glycol (PEG) as the connecting agents between Fe_3O_4 spheres and glucose. Moreover, the influence of reaction time and the used amount of reactants on the final morphology of the products were investigated. The formed product has a well core−shell structure, which can be evenly coated with nearly monodispersed Pd NPs. Compared to commercially used Pd/C catalyst, the as-synthesized catalyst exhibits a higher catalytic activity and better recyclability toward the reduction of organic dye such as methyl orange (MO). Its catalytic activity toward the hydrogenation of allyl alcohol was also investigated and compared to Pd/C.

2. EXPERIMENTAL SECTION

2.1. Materials. All the reagents were of analytical grade and used without further purification including $PdCl_2$ (Aldrich), $FeCl_3 \cdot 6H_2O$, $FeCl_2 \cdot 4H_2O$, anhydrous sodium acetate (NaAc), glucose, PEG (M_w = 1500 and 20 000), ethylene glycol, ethanol, MO, concentrated nitric acid (HNO_3), concentrated HCl, and allyl alcohol. The water used in the experiments was distilled water.

2.2. Preparation of Fe_3O_4 Microspheres. The Fe_3O_4 microspheres were prepared according to Li's method (16). The detailed process is as follows: $FeCl_3 \cdot 6H_2O$ (1.08 g, 4 mmol) was dissolved in ethylene glycol (40 mL) to form a clear solution, followed by the addition of NaAc (2.88 g) and PEG (0.8 g, M_w = 20 000). The mixture was stirred vigorously for 30 min and then sealed in a teflon-lined stainless-steel autoclave (40 mL capacity). The autoclave was heated to and maintained at 200 °C for 8 h, and then allowed to cool to room temperature. The black products were washed several times with ethanol and dried at 60 °C for 6 h.

2.3. Preparation of Fe_3O_4@C Microspheres. In a typical experiment, Fe_3O_4 microspheres (0.05 g), glucose (4 g) and PEG (0.5 g, M_w = 1500) were dispersed in distilled water (20 mL) by ultrasonicating for 15 min. The mixture was stirred for 30 min and then sealed in a teflonlined stainless-steel autoclave (40 mL capacity). The autoclave was heated to and maintained at 180 °C for 12 h, and then allowed to cool to room temperature. The black products were separated by externally applied magnetic field and washed several times with water and ethanol. Finally, they were dried at 60 °C for 6 h.

2.4. Preparation of Pd NP-Loaded Fe_3O_4@C Nanospheres. Fe_3O_4@C microspheres (50 mg) were dispersed in absolute ethanol (25 mL) after ultrosonicating them for 20 min. $PdCl_2$ (11.1 mg) was then added into the above suspension, followed by reacting at 70 °C for 20 min under vigorous stirring. After the reaction, the product was separated by externally applied magnetic field, washed with distilled water twice, and dried at 60 °C for 6 h.

2.5. Characterization. Scanning electron microscopy (SEM) measurements were performed on a SHIMADZU SSX-550 microscope. Transmission electron microscopy (TEM) experiments were performed on Hitachi 800 (Tokyo, Japan) and JEM-1200 EX (JEOL) electron microscopes with an acceleration voltage of 200 kV. Fourier transform infrared (FTIR) spectra of KBr powder-pressed pellets were recorded on a BRUKER VECTOR 22 Spectrometer. X-ray diffraction (XRD) patterns were obtained with a Siemens D5005 diffractometer using CuKα radiation. Analysis of the X-ray photoelectron spectra (XPS) was performed on an ESCLAB MKII using Al as the exciting source. The room-temperature magnetization in the applied magnetic field was performed by model JDM-13 vibrating sample magnetometer (VSM). Inductively coupled plasma atomic spectrum (ICP) was performed on Perkin-Elmer OPTIMA 3300DV. Ultraviolet−visible spectra (UV−vis) were recorded on a Shimadzu UV-2501 PC spectrometer.

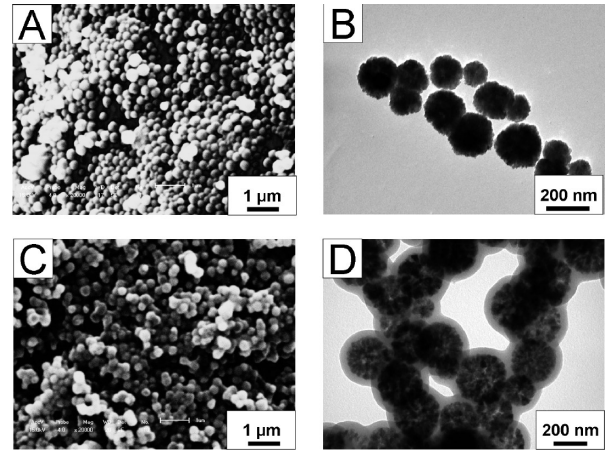

FIGURE 1. SEM and TEM images of (A, B) Fe_3O_4 and (C, D) Fe_3O_4@C microspheres.

2.6. Catalytic Activity Measurements. 2.6.1. *Catalytic Reduction of MO.* As a model reaction, we compared the catalytic activity of the final product with commercially used Pd/C catalyst on the reduction of MO by $NaBH_4$. In a typical run, catalyst aqueous solution (0.02 mL) was added to a mixture of MO (1.5 mL, 0.2 mM) and $NaBH_4$ (1.5 mL, 30 mM). The final concentration of Pd in the MO solution was kept constant (0.015 mg/mL) and the absorption spectra of the reaction solution were recorded at different times after the addition of the catalyst.

When the catalytic reaction was completed, the Fe_3O_4@C/Pd spheres were separated by externally applied magnetic field. Then they were ultrasonicated in HNO_3 aqueous solution (1M) for 5 min to remove the absorbed dye. After that, they were reused in the catalytic reaction. The recyclability of the as-synthesized catalyst was determined by measuring the degradation time when the MO was fully degraded.

2.6.2. *Catalytic Hydrogenation of Allyl Alcohol.* Acrylic acid (10.0 mmol), Fe_3O_4@C/Pd catalyst (10.6 mg containing 2 μmol Pd), and methanol (30.0 mL) were introduced into a 50 mL reaction vessel. The catalytic reaction was carried out at 303 K under a constant hydrogen pressure (1.0 MPa) and stirring. A sample was withdrawn at a regular interval and analyzed by Gas Chromatography (GC-6890) equipment with flame-ionization detector and 30 m capillary column (HPINNOWAX). Yield was determined by the following equation: yield = [area of product]/[area of substrate + area of product] (17−19). As control, the hydrogenation was also carried out by using 5% Pd/C as catalysts (4.3 mg containing 2 μmol Pd).

3. RESULTS AND DISCUSSION

3.1. Formation Mechanism and Morphology. Compared to Fe_3O_4 microspheres (Figure 1A,B), it can be seen that when the reaction time was 12 h, uniform Fe_3O_4@C spheres (Figure 1C,D) with diameters mainly between 280 and 350 nm could be obtained and the

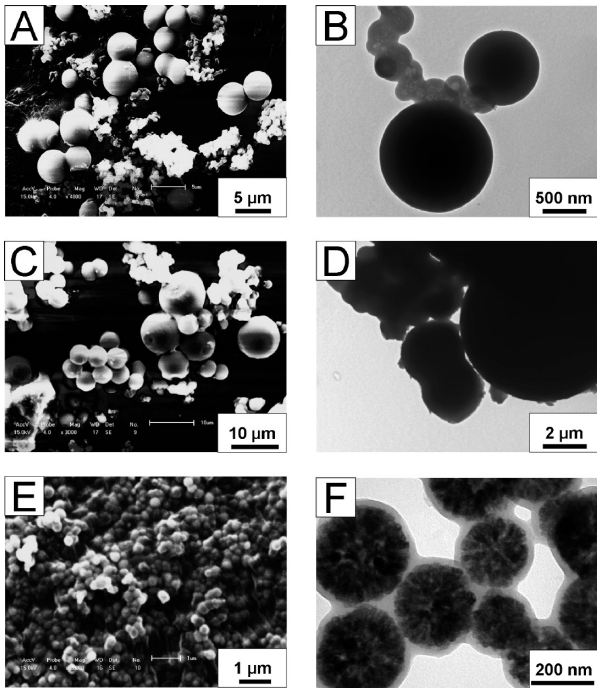

FIGURE 2. SEM and TEM images of Fe_3O_4@C microspheres: (A, B) reacting for 24 h; (C, D) without PEG and (E, F) with double amount of PEG.

thickness of the carbon layer was 55−60 nm which was much thicker than those reported by other groups (14). To get Fe_3O_4@C microspheres with uniform size and well morphology, the influence of the reaction time and the added amount of PEG to the final morphology of the products was investigated. When the reaction time was prolonged to 24 h, Fe_3O_4 cores were dissolved and big carbon spheres (1−5 μm) appeared (Figure 2A,B). Such results were caused by the long-term carbonization of the polysaccharide layer during which acid would be released in the center of such spheres. The accurate form of such acid is not clear yet but according to the transformation process from polysaccharide to carbon layer, only carbon, oxygen, and hydrogen atoms could leave the polymer chain and form the acid. As a result, such acid may be organic carboxylic acid or inorganic carbonic acid. To further confirm the form of the released acid, we filtered the supernatant after reaction and added it into 1 M $CaCl_2$ solution. However, as no precipitate was formed, the acid was not inorganic carbonic acid. Moreover, the filtered supernatant was also dropped on a KBr pellet to see its infrared spectrum (curve d in Figure 6A). As the peaks at 1718, 1666, and 2923 cm^{-1} that were attributed to C═O, C═C, and CO−H and the bands in the range of 1000−1300 cm^{-1} that corresponded to C−O stretching and O−H bending vibrations can be observed, it might be concluded that the acid should be some kind of organic carboxylic acid. The longer the carbonization process lasted, the more the acid would be released in the mixture. On the other hand, according to our experimental results, the appearance of big carbon spheres was mainly caused by the quick aggregation and deposition of the polysaccharide layer. As reported before, polysaccharide first formed in the mixture and then deposited onto the spheres (12). When the reaction time was shorter than 12 h, the amount of polysaccharide in the mixture was fewer and its deposition proceeded in a mild and controllable way. However, when the reaction proceeded further, more and more polysaccharide would form in the mixture and reach an oversaturation state. At this time, excess polysaccharide would aggregate into pure carbon spheres, which would then grow in a fast and uncontrollable way, leading to big carbon spheres. As reported in the experimental section, after the reaction, the slurry was placed under externally applied magnetic field to separate the product and the supernatant. It was found that the supernatant separated from the mixture after reacting for 24 h was in deeper brown than that after reacting for 12 h, indicating that more polysaccharide formed.

The amount of PEG used in the reaction was then tuned to see its influence on the final morphology of the composite spheres. As shown in Figure 2, when no PEG was used in the reaction, Fe_3O_4 spheres could only be wrapped with a thin carbon layer and most of the polysaccharide aggregated to form big carbon spheres. This was due to the weak interaction between Fe_3O_4 surface and glucose-based materials. Further doubling the amount of PEG would lead to Fe_3O_4@C microspheres with similar morphology to those obtained under normal conditions, indicating that PEG played an important role in shaping the core−shell structure as the connecting agent. This was due to the unique sticky property of amphiphilicity PEG to Fe_3O_4 spheres and polysaccharide. Finally, it tightly bound glucose-based polysaccharide to the surface of Fe_3O_4 spheres and a well core−shell structure was prepared.

In our work, the added amounts of Fe_3O_4 nanospheres and glucose were also tuned in order to control the thickness of the carbon layer. However, the thickness was not controllably tuned as we expected. When the used amount of Fe_3O_4 microspheres was halved, only a few hollow carbon spheres and a lot of big aggregated carbon spheres instead of core−shell Fe_3O_4@C spheres could be observed (Figure 3). The morphology was similar to those when the reaction time was prolonged to 24 h and could be explained in the same way. In detail, as the Fe_3O_4 seeds were fewer in the mixture, the formed polysaccharide was excessive and hence self-aggregated into big carbon spheres. Moreover, the carbonization of excessive polysaccharide on Fe_3O_4 spheres would produce more acid and finally the Fe_3O_4 cores were dissolved. In conclusion, we could not get Fe_3O_4@C spheres with thicker carbon layer by halving the used amount of Fe_3O_4 spheres but we could get Fe_3O_4@C spheres with thinner carbon layer by doubling the used amount of Fe_3O_4 spheres (Figure 3C,D). Similar results could be obtained by changing the used amount of glucose. Figure 3E,F showed that halving the amount of glucose could get Fe_3O_4@C spheres with thinner carbon layer, while doubling the amount of glucose could only get big carbon spheres with a few Fe_3O_4@C spheres. However, Fe_3O_4 cores were not dissolved, though more glucose was used. This might because that the explosive formation of carbon spheres happened.

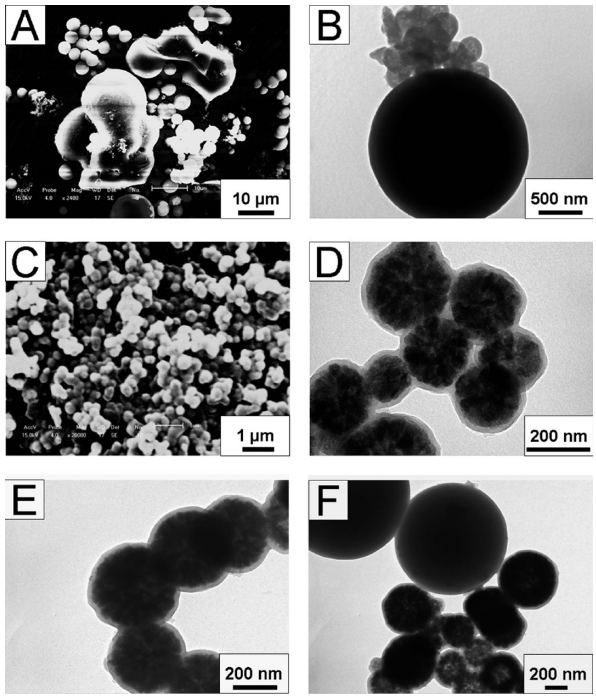

FIGURE 3. SEM and TEM images of Fe_3O_4@C microspheres: (A, B) with half amount of Fe_3O_4 microspheres; (C, D) with double amount of Fe_3O_4 microspheres; (E) with half amount of glucose; and (F) with double amount of glucose.

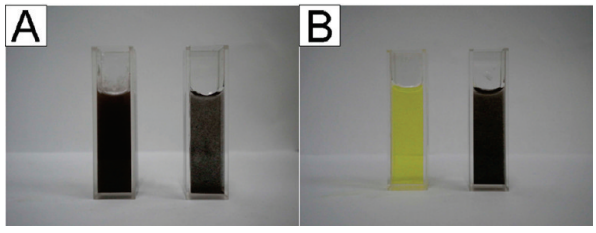

FIGURE 4. Photographs of Fe_3O_4 (left) and Fe_3O_4@C (right) microspheres (A) before and (B) after acid treatment.

Therefore, less polysaccharide was absorbed onto the surface of Fe_3O_4 microspheres, resulting in less acid releasing in the center of Fe_3O_4 microspheres. Accordingly, Fe_3O_4 cores were reserved. In conclusion, the thickness of the carbon layer could be easily tuned to a small value by controlling the amounts of the reactants. However, it was difficult to get a thicker layer because the self-aggregation of polysaccharide would always happen instead of deposition to the Fe_3O_4@C microspheres.

Once the Fe_3O_4@C microspheres were formed, they could be stable in a relatively acid environment. The Antiacid ability of the Fe_3O_4@C composite microspheres was investigated and compared to pure Fe_3O_4 microspheres by ultrasonicating them in 1 M HCl solution at 45−50 °C for 70 min. After the acid treatment, pure Fe_3O_4 microspheres were fully dissolved and their dispersion turned to light yellow which was the color of Fe^{3+} ions (left in Figure 4A,B). However, the dispersion of Fe_3O_4@C composite spheres did not exhibit much change (right in Figure 4A,B). ICP results showed that the weight percentages of Fe_3O_4 in Fe_3O_4@C composite microspheres before and after the acid treatment were 16.61 and 14.23%, respectively. This means that only about

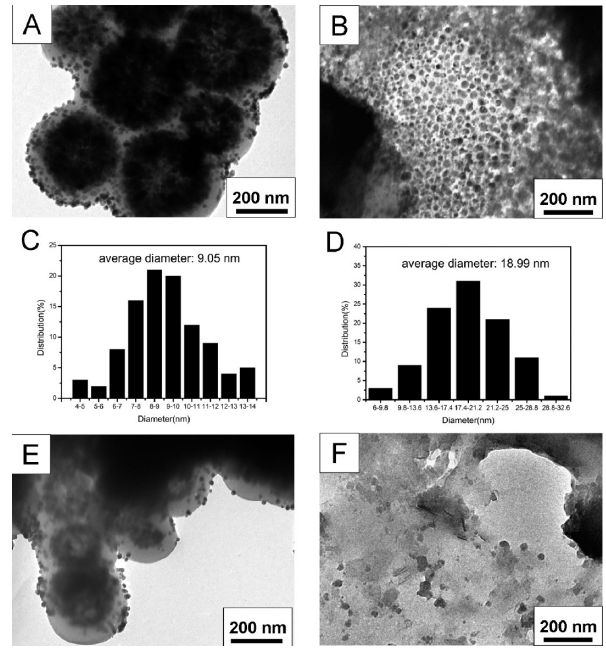

FIGURE 5. TEM image of (A) Fe_3O_4@C/Pd microspheres and (B) Pd/C before catalytic reaction; size distribution of (C) Fe_3O_4@C/Pd microspheres and (D) Pd/C; TEM image of (E) Fe_3O_4@C/Pd microspheres and (F) Pd/C after catalytic reaction.

16.7% of the Fe_3O_4 cores were dissolved and 83.3% were reserved. This superior antiacid ability of the Fe_3O_4@C composite microspheres was due to the protection by the thick and dense carbon layer coated onto the Fe_3O_4 cores.

The as-prepared Fe_3O_4@C nanospheres could act as magnetic supports for palladium NPs because the carbon layer has a lot of reductive groups on their surface. After the in situ reduction process was carried out, nearly monodispersed Pd NPs (6−12 nm) were evenly grown on the surface of Fe_3O_4@C microspheres (Figure 5A). ICP result showed that the weight percentage of Pd in the final product was about 2%. The morphology and size distribution of the Pd NPs in our product were also compared with those of Pd NPs in commercially used Pd/C catalyst. According to Figure 5, it could be observed that the Pd NPs loaded on Fe_3O_4@C microspheres have a smaller average diameter (9.05 nm) than those on Pd/C (18.99 nm).

3.2. Structural Characterization of Fe_3O_4@C and Fe_3O_4@C/Pd Microspheres. In order to confirm the existence and the kinds of these surface groups, FTIR spectra of Fe_3O_4, Fe_3O_4@C and Fe_3O_4@C/Pd spheres were performed in Figure 6A. As shown, the spectra of Fe_3O_4@C and Fe_3O_4@C/Pd spheres exhibited similar peaks at 1706 and 1612 cm^{-1}, which were attributed to C═O and C═C vibrations, respectively, supporting the concept of aromatization of glucose during hydrothermal treatment. Moreover, the bands in the range 1000−1300 cm^{-1} were corresponding to C−O stretching and O−H bending vibrations, implying the existence of a large number of residual hydroxyl groups on their surface (12).

Raman spectra of Fe_3O_4@C and Fe_3O_4@C/Pd spheres were performed to investigate the structure of the carbon layer. The two curves in Figure 6B showed two strong peaks

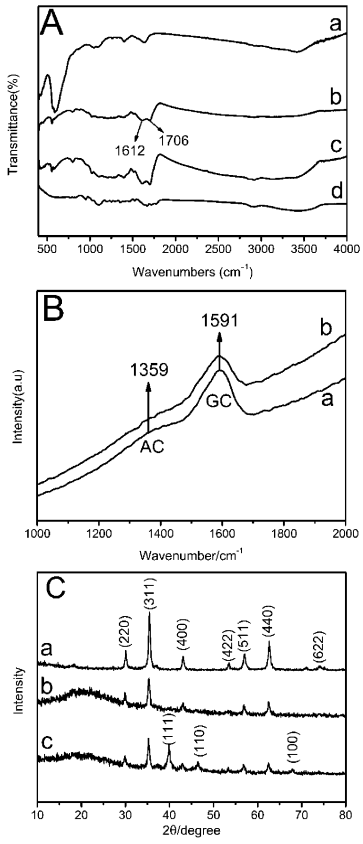

FIGURE 6. (A) FTIR spectra of (a) Fe_3O_4, (b) Fe_3O_4@C, (c) Fe_3O_4@C/Pd microspheres, and (d) the supernatant after preparation of Fe_3O_4@C. (B) Raman spectra of (a) Fe_3O_4@C, (b) Fe_3O_4@C/Pd microspheres. (C) XRD spectra of (a) Fe_3O_4, (b) Fe_3O_4@C, (c) Fe_3O_4@C/Pd microspheres.

at 1591 and 1359 cm^{-1}, which were attributed to in-plane vibrations of crystalline graphite and disordered amorphous carbon, respectively (12). The relatively higher peak at 1591 cm^{-1} indicated that the carbon layer made from glucose had an ordered, graphitelike structure, whereas the disordered peak at 1359 cm^{-1} might originate from the defects on the surface of carbon layer.

From the XRD spectra of all the samples in Figure 6C, the characteristic diffraction peaks of Fe_3O_4 at $2\theta = 29.91$, 35.41, 43.11, 57.21, and 62.81° could be observed and were well-indexed to the cubic spinel structured magnetite (JCPDS file No.19−0629) (20), indicating that the crystallite phase of Fe_3O_4 can be well-preserved during the reaction. After the coating process, a wide peak centered at $2\theta = 20.55°$ was observed, indicating that the carbon matrix was amorphous (13). Finally, the characteristic diffraction peaks of Pd at $2\theta = 40.1$, 46.6, and 68.1°, which corresponded to (111), (110), and (100) crystalline planes of Pd (JCPDS 5−0683) (21) were observed in the spectrum of Fe_3O_4@C/Pd spheres, indicating that Pd element existed in the form of Pd^0, not Pd^{2+}.

To further confirm that in our product, the Fe_3O_4 core has been fully wrapped by the carbon layer, we performed XPS spectra to show their surface elements (Figure 7). Compared with Figure 7A, the characteristic peak of Fe element absolutely disappeared after the coating of carbon layer (Figure 7B). In addition, after the loading of Pd NPs, the sharp peaks

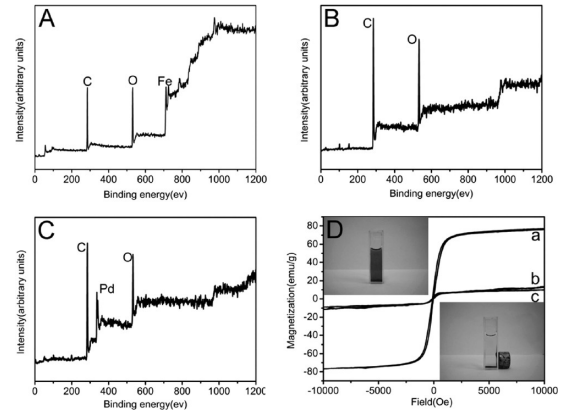

FIGURE 7. XPS spectra of (A) Fe_3O_4, (B) Fe_3O_4@C, and (C) Fe_3O_4@C/Pd microspheres. (D) Magnetization vs applied magnetic field at room temperature for: (a) Fe_3O_4, (b) Fe_3O_4@C, and (c) Fe_3O_4@C/Pd microspheres. Inset in D shows the photographs of the dispersion of Fe_3O_4@C/Pd microspheres before (above) and after (below) magnetic separation.

centered at 341.5 and 335.7 eV appeared (Figure 7C), again verifying that the existing form of Pd elements was Pd^0.

The magnetic properties of the obtained composite spheres were investigated with a VSM. Typical magnetization curves as a function of the applied field at room temperature (300K) were shown in Figure 7D. The saturation magnetization decreases from 76.8 to 13.0 and 9.7 emu g^{-1} along with the increase of coating materials. ICP results show that the weight percentage of Fe_3O_4 in Fe_3O_4@C and Fe_3O_4@C/Pd composite sphere are 16.61 and 13.32%, respectively, which are approximately proportional to their saturation magnetization. All the samples exhibit a magnetic coercivity of about 136 Oe because the sizes of Fe_3O_4 spheres already exceed the critical size of a single magnetic domain (22).

The Fe_3O_4@C/Pd composite sphere could be easily separated by externally applied magnetic field. As shown in the insert images in Figure 7D, the black particles were attracted toward the magnet in a very short time, which provides an easy and efficient way to separate and recycle the materials from heterogeneous reaction systems.

3.3. Catalytic Activity and Recyclability of Fe_3O_4@C/Pd Composite Microspheres toward the Reduction of MO. We have investigated the catalytic activity and recyclability of Fe_3O_4@C/Pd composite microspheres and compared them with commercially used Pd/C (5%) catalyst. As the reduction of MO with $NaBH_4$ could be easily monitored by UV−vis absorption spectroscopy without the formation of any appreciable byproduct, it was selected as the model reaction which proceeded quite slowly in the absence of catalyst (23). From Figure 8, it can be observed that the spectrum of the mixture of the MO and $NaBH_4$ solution was dominated by the band at 464.5 nm, which corresponded to intermolecular charge transfer for MO. The intensity of this characteristic band decreases very little after 12 h. To confirm that the decrease in the characteristic band of MO in the presence of Fe_3O_4@C/Pd was caused by the catalytic reduction of MO, not the adsorption of MO by the carbon layer, we also performed the UV−vis

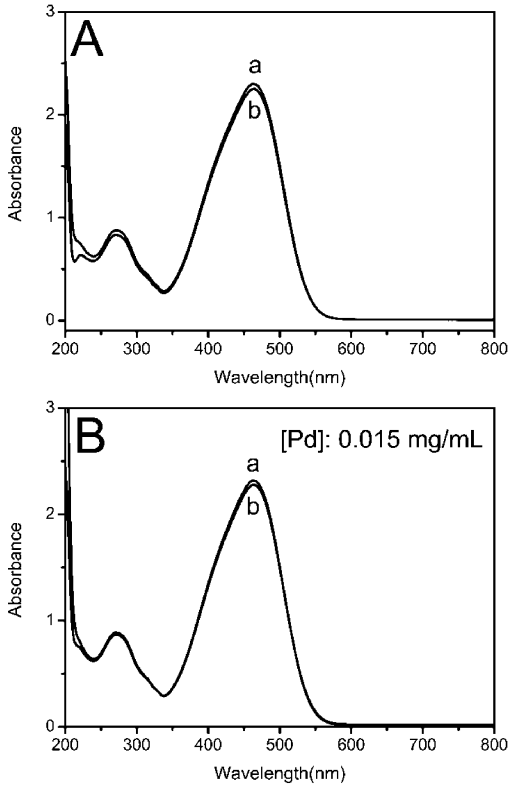

FIGURE 8. (A) Absorption spectra of MO and $NaBH_4$ mixed aqueous solution after (a) 1 min and (b) 12 h. (B) Absorption spectra of MO aqueous solution (a) before and (b) after addition of Fe_3O_4@C/Pd aqueous dispersion for 12 h.

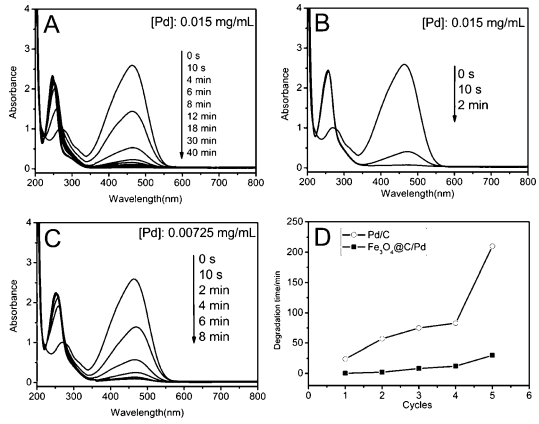

FIGURE 9. Successive absorption spectra of aqueous solution containing MO and $NaBH_4$ after the addition of (A) Pd/C and (B, C) Fe_3O_4@C/Pd aqueous dispersion. The concentration of Pd in the mixed solution is 0.015 mg/mL in A and B, whereas it is 0.0725 mg/mL in C. (D) Reduction time of MO in five successive cycles with Pd/C catalyst and Fe_3O_4@C/Pd microspheres.

spectra of MO solution before and after adsorbed by Fe_3O_4@C/Pd for 12 h in Figure 8B. The results showed that very few MO can be adsorbed by the carbon layer in the catalyst. As a result, MO reduction is a suitable reaction to evaluate the activity of the prepared catalyst. In Figure 9, the successive absorption spectra of the reduction of MO catalyzed by Pd/C (Figure 9A) showed that after the addition of Pd/C catalyst, the reduction reaction of MO was accelerated and completed after 40 min. Compared to Pd/C, in the presence of as-synthesized Fe_3O_4@C/Pd composite spheres, the band at 464.5 nm decreased a lot more quickly and totally disappeared after only 2 min (Figure 9B). In panels A and B in Figure 9, the used Pd content in the mixed solution was 0.015 mg/mL for both Pd/C catalyst and Fe_3O_4@C/Pd composite spheres. Using Fe_3O_4@C/Pd as the catalyst, even when the Pd content was tuned to 0.00725 mg/mL in the mixed solution, the reduction still proceeded very fast and was completed after only 8 min. The results indicated that the catalytic activity of Fe_3O_4@C/Pd composite microspheres was superior to Pd/C catalyst. This may be due to the fact that in our products, Pd NPs with smaller average size were evenly dispersed on the Fe_3O_4@C surface. Comparatively, as reported by Corma et al., the average diameter of Pd NPs in Pd/C was 14.52 nm (24). Similarly, from Figure 5, we can observe that the average diameter of Pd NPs in Pd/C used here was 18.99 nm. As a result, the catalyst of Fe_3O_4@C/Pd composite microspheres had larger surface area, which could offer more catalytic sites toward the reduction of MO than Pd/C catalyst.

More detailed information about the catalytic activity of the composites is known by studying the kinetics of the reduction reaction. The sodium borohydride in the reactive system is requested to greatly exceed the content of MO, so that the rates of the reduction are assumed to be independent of the concentration of sodium borohydride, and thus the kinetics of the reduction could be treated as pseudo-first-order in MO concentration (25, 26). The ratio of absorbance A_t of MO at time t to its value A_0 measured at $t = 0$ directly gives the corresponding concentration ratios C_t/C_0 of MO. Thus the kinetic equation of the reduction could be shown as $dC_t/dt = K_{app}t$ or $\ln(C_0/C_t) = \ln(A_0/A_t) = K_{app}t$, where C_t is the concentration of MO at time t and K_{app} is the apparent rate constant, which can be obtained from the decrease of peak intensity at 464.5 nm with time.

According to the above equation, the relations of $\ln(C_0/C_t)$ versus time t can be obtained. By calculating the slope of the fitting line, a value of K_{app} is obtained which is 1.44 to Fe_3O_4@C/Pd, whereas it is 0.26 to Pd/C. A higher value of K_{app} means higher catalytic activity of the catalyst. According to the results, we can calculate the approximate time to reduce a certain amount of MO.

The immobilization of Pd NPs with magnetic support may render them a practical recyclable nanocatalyst. As a recyclable catalyst, another important factor, the renewable catalytic activity, was also investigated by performing the MO reduction five times using the recycled composite nanocatalysts. The catalytic activity of the recycled composite nanocatalysts was characterized by the reaction time when the reduction was fully completed. For comparison, Pd/C was also separated by centrifuging and recycled in the reductive reaction. The used Pd content in the mixed solution was 0.02 mg/mL and was kept the same for both Pd/C catalyst and Fe_3O_4@C/Pd composite microspheres in the recycling experiments. After each cycle, the catalysts were ultrasonicated in 1 M HNO_3 aqueous solution for 5 min to remove the absorbed MO and its leuco form on the catalysts. As clearly shown in Figure 9D, the reduction time after each cycle was 10 s, 2,

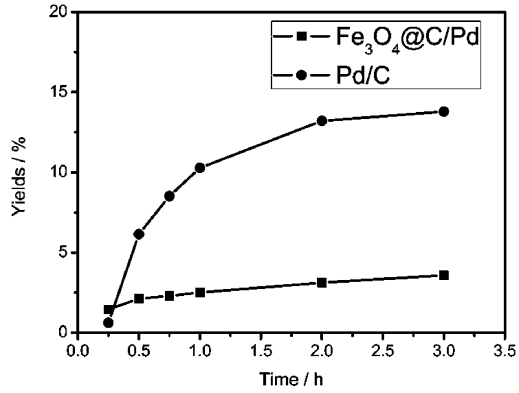

FIGURE 10. Hydrogenation of allylic alcohol using Pd/C or Fe_3O_4@C/Pd as the catalyst.

8, 12, and 30 min for Fe_3O_4@C/Pd composite microspheres, whereas it was 24, 57, 75, 83, and 210 min for Pd/C catalyst. The increasing trend of the reduction time could be observed for both Fe_3O_4@C/Pd composite spheres and Pd/C catalyst. The reduction time was prolonged after each cycle because the loss of the catalyst might happen during its reclamation. More importantly, the aggregation of the Pd NPs might also happen after each cycle, and thus the surface area of the catalyst as well as the catalytic sites were decreased. However, it was obvious that as-synthesized Fe_3O_4@C/Pd composite spheres exhibited superior renewable catalytic activity than Pd/C catalyst. According to our observation, two reasons were suggested to explain the phenomenon. First, as the Fe_3O_4@C/Pd composite spheres were reclaimed by external magnetic field, the loss of them was very few. On the other hand, as reported above, the abundant functional groups on the surface of the carbon layer could tightly bind the Pd NPs and efficiently prevent them from leaching and aggregating which can be confirmed by the TEM images of Fe_3O_4@C/Pd microspheres and Pd/C before and after catalytic reaction (Figure 5). According to the two unique properties of Fe_3O_4@C/Pd composite microspheres, their catalytic activity was better reserved after each cycle than Pd/C catalyst.

Furthermore, the catalytic activity of our product toward the hydrogenation of olefin (allyl alcohol) was also investigated and compared to Pd/C (5%) catalyst (see Figure 10). However, in contrast to the reduction of MO, Fe_3O_4@C/Pd exhibited lower catalytic activity than Pd/C. After reacting for 4 h, the yield of reaction product propanol was 3.58% when using Fe_3O_4@C/Pd as catalyst, whereas the value was 13.79% when using Pd/C as the catalyst. This might be due to the porous active carbon having higher hydrogen adsorption and storage capacity that favored the catalytic hydrogenation of allyl alcohol. This also inspires us to do more work to control the morphology of the outer carbon layer to be a porous structure in the future to enhance its catalytic activity toward the hydrogenation of olefins.

4. CONCLUSIONS

In conclusion, novel Fe_3O_4@C hybrid microspheres using glucose as the carbon source were constructed and used as the support for catalytic noble metal NPs. In catalysis, these nanocomposites provided not only large surface areas for high loading of catalysts but also the ability to be easily separated from the reaction mixture by externally applied magnetic field. Furthermore, the thick carbon layer could efficiently prevent the Fe_3O_4 cores from being dissolved by acid. The prepared Fe_3O_4@C/Pd composite microspheres were then used in the catalysis of the reduction of MO and the results showed that they had enhanced catalytic activity and renewable catalytic activity when compared with commercially used Pd/C catalyst. This environmentally friendly magnetic carrier has more potential applications in the life and materials science such as drug delivery, ferrofluids (27), magnetic storage media, stem cell labeling, and magnetic resonance imaging (MRI) (28−30). Finally, the method of coating carbon layer on inorganic cores can be applied to other inorganic materials to obtain multifunctional composite spheres.

Acknowledgment. The financial support from the National 973 project (2007CB936203), and the National Nature Science Foundation of China (50973038 and 20904015) are greatly appreciated.

REFERENCES AND NOTES

(1) Lvov, Y. M.; Shchukin, D. G.; Mohwald, H.; Price, R. R. *Acs Nano* **2008**, *2*, 814–820.
(2) Deng, Y. H.; Qi, D. W.; Deng, C. H.; Zhang, X. M.; Zhao, D. Y. *J. Am. Chem. Soc.* **2008**, *130*, 28–29.
(3) Xu, X. Q.; Deng, C. H.; Gao, M. X.; Yu, W. J.; Yang, P. Y.; Zhang, X. M. *Adv. Mater.* **2006**, *18*, 3289–3293.
(4) Park, J.; An, K.; Hwang, Y.; Park, J. G.; Noh, H. J.; Kim, J. Y.; Park, J. H.; Hwang, N. M.; Hyeon, T. *Nat. Mater.* **2004**, *3*, 891–895.
(5) Mori, K.; Kondo, Y.; Morimoto, S.; Yamashita, H. *J. Phys. Chem. C* **2008**, *112*, 397–404.
(6) Zhu, A. P.; Yuan, L. H.; Dai, S. *J. Phys. Chem. C* **2008**, *112*, 5432–5438.
(7) Lu, X. F.; Mao, H.; Zhang, W. J. *Polym. Composite.* **2009**, *30*, 847–854.
(8) Kim, J.; Lee, J. E.; Lee, J.; Yu, J. H.; Kim, B. C.; An, K.; Hwang, Y.; Shin, C. H.; Park, J. G.; Kim, J.; Hyeon, T. *J. Am. Chem. Soc.* **2006**, *128*, 688–689.
(9) Zhu, Y. F.; Kockrick, E.; Ikoma, T.; Hanagata, N.; Kaskel, S. *Chem. Mater.* **2009**, *21*, 2547–2553.
(10) Xuan, S. H.; Wang, Y. X. J.; Yu, J. C.; Leung, K. C. F. *Langmuir* **2009**, *25*, 11835–11843.
(11) Wang, Q.; Li, H.; Chen, L. Q.; Huang, X. J. *Carbon* **2001**, *39*, 2211–2214.
(12) Sun, X. M.; Li, Y. D. *Angew. Chem., Int. Ed.* **2004**, *43*, 597–601.
(13) Cakan, R. D.; Titirici, M. M.; Antonietti, M.; Cui, G. L.; Maier, J.; Hu, Y. S. *Chem. Commun.* **2008**, *32*, 3759–3761.
(14) Wang, Z. F.; Guo, H. S.; Yu, Y. L.; He, N. Y. *J. Magn. Magn. Mater.* **2006**, *302*, 397–404.
(15) Zhang, Z. B.; Duan, H. F.; Li, S. H.; Lin, Y. J. *Langmuir* **2010**, *26*, 6676–6680.
(16) Deng, H.; Li, X. L.; Peng, Q.; Wang, X.; Chen, J. P.; Li, Y. D. *Angew. Chem., Int. Ed.* **2005**, *44*, 2782–2785.
(17) Wu, H.; Wu, C.; He, Q.; Liao, X. P.; Shi, B. *Mater. Sci. Eng., C* **2010**, *30*, 770–776.
(18) Huang, X.; Li, L.; Liao, X. P.; Shi, B. *J. Mol. Catal. A: Chem.* **2010**, *320*, 40–46.
(19) Mori, K.; Yoshioka, N.; Kondo, Y.; Takeuchib, T.; Yamashita, H. *Green Chem.* **2009**, *11*, 1337–1342.
(20) Yu, X. G.; Wan, J. Q.; Shan, Y.; Chen, K. Z.; Han, X. D. *Chem. Mater.* **2009**, *21*, 4892–4898.
(21) Chang, G.; Oyama, M.; Hirao, K. *J. Phys. Chem. B* **2006**, *110*, 20362–20368.
(22) Li, Z.; Sun, Q.; Gao, M. Y. *Angew. Chem., Int. Ed.* **2005**, *44*, 123–126.

(23) Yang, S. C.; Hong, F.; Wang, L. Q.; Guo, S. W.; Song, X. P.; Ding, B. J.; Yang, Z. M. *J. Phys. Chem. C* **2010**, *114*, 203–207.
(24) Corma, A.; Garcia, H.; Leyva, A. *J. Mol. Catal. A: Chem.* **2005**, *230*, 97–105.
(25) Mei, Y.; Lu, Y.; Polzer, F.; Ballauff, M.; Drechsler, M. *Chem. Mater.* **2007**, *19*, 1062–1069.
(26) Wang, Y.; Wei, G.; Zhang, W.; Jiang, X.; Zheng, P.; Shi, L.; Dong, A. *J. Mol. Catal. A* **2007**, *266*, 233–238.
(27) Sun, S. H.; Zeng, H. *J. Am. Chem. Soc.* **2002**, *124*, 8204–8205.
(28) Park, J. I.; Jun, Y. W.; Choi, J. S.; Cheon, J. *Chem. Commun.* **2007**, *47*, 5001–5003.
(29) Hultman, K. L.; Raffo, A. J.; Grzenda, A. L.; Harris, P. E.; Brown, T. R.; O'Brien, S. *Acs Nano* **2008**, *2*, 477–484.
(30) Shi, X. Y.; Wang, S. H.; Swanson, S. D.; Ge, S.; Cao, Z. Y.; Antwerp, M. E. V.; Landmark, K. J., Jr.; Baker, J. R. *Adv. Mater.* **2008**, *20*, 1671–1678.

AM101077A